Analytical model to predict the effect of a finite impedance surface on the propagation properties of 2D Sonic Crystals

2011 J. Phys. D: Appl. Phys. 44 265501

(http://iopscience.iop.org/0022-3727/44/26/265501)

IOP PUBLISHING JOURNAL OF PHYSICS D: APPLIED PHYSICS

J. Phys. D: Appl. Phys. **44** (2011) 265501 (12pp) doi:10.1088/0022-3727/44/26/265501

Analytical model to predict the effect of a finite impedance surface on the propagation properties of 2D Sonic Crystals

V Romero-García[1,2], J V Sánchez-Pérez[2] and L M Garcia-Raffi[3]

[1] Instituto de Ciencia de Materiales de Madrid, Consejo Superior de Investigaciones Científicas, Spain
[2] Centro de Tecnologías Físicas: Acústica, Materiales y Astrofísica, Universidad Politécnica de Valencia, Spain
[3] Instituto Universitario de Matemática Pura y Aplicada, Universidad Politécnica de Valencia, Spain

E-mail: virogar1@gmail.com

Received 18 February 2011, in final form 28 April 2011
Published 13 June 2011
Online at stacks.iop.org/JPhysD/44/265501

Abstract
The use of sonic crystals (SCs) as environmental noise barriers has certain advantages from both the acoustical and the constructive points of view with regard to conventional ones. However, the interaction between the SCs and the ground has not been studied yet. In this work we are reporting a semi-analytical model, based on the multiple scattering theory and on the method of images, to study this interaction considering the ground as a finite impedance surface. The results obtained here show that this model could be used to design more effective noise barriers based on SCs because the excess attenuation of the ground could be modelled in order to improve the attenuation properties of the array of scatterers. The results are compared with experimental data and numerical predictions thus finding good agreement between them.

(Some figures in this article are in colour only in the electronic version)

1. Introduction

Periodic arrangements of scatterers embedded in a medium with different physical properties show ranges of frequencies, known as band gaps (BGs), where the transmission of waves is forbidden. If these periodic systems are formed by a combination of solids and fluids then they are usually called sonic crystals (SCs) [1]. In the last years, an increasing interest has appeared in the potential exploitation of SCs as environmental noise barriers [2–4].

Some examples of the advantages of using SCs instead of conventional screens are the reduction in the size of the foundation or the possibility of designing specific screens for predetermined conditions. However, the acoustical properties of SCs depend on several factors showing some particularities in their attenuation properties. For example, the size and position of the BGs depend on several factors such as the direction of incidence of the wave on the SCs and the type of arrangement of the scatterers [5]. As a consequence, the development of the screens based on SCs is not a trivial process.

In order to avoid these handicaps several works have been intensively developed in last years. The use of both materials with acoustical properties added or more efficient distribution of scatterers are two examples. The use of resonators [6] or absorbent materials [7, 8] in the first case, and the use of quasi-ordered [9, 10] or quasi-fractal [11] structures in the second case have been studied.

The existence of the ground is one of the factors to be considered in the use of SCs as noise barriers. Up to now one of the most appropriate analytical approaches to predicting the transmission properties of finite SCs has been based on the well-known multiple scattering theory (MST) [12–15], which is a self-consistent method to calculate the acoustic pressure including all orders of scattering considering the superpositions of the solution for a simple scatterer. MST has been used to predict the acoustical performance of SCs

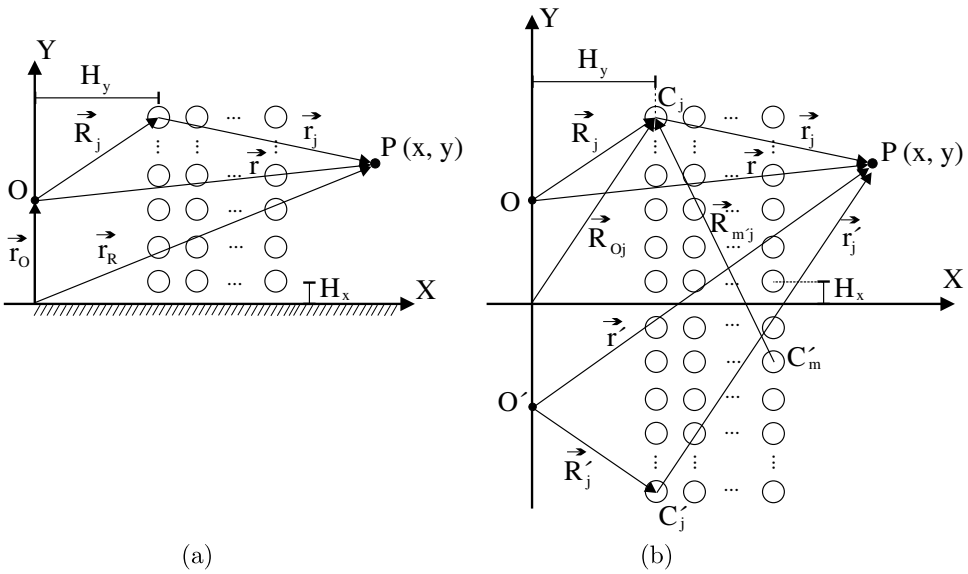

Figure 1. (*a*) Square lattice array above a perfectly reflecting plane. (*b*) Schematic of the real and the image sources and the real and the image scatterers.

in the absence of a ground plane [15]. On the other hand, some works use MST to study the possibility of modulating the scattering using a ground made of random [16] or periodic inclusions [17]. However, the interaction between the SCs and the ground has not been studied yet, and in this case the MST is an unrealistic approximation as the presence of the ground should be considered.

In this work, we present a semi-analytical method based on both the MST and the method of images [16, 18] to study the effect of ground planes on the propagation properties of a SC made of rigid scatterers embedded in air. Two types of grounds, acoustically rigid and with finite impedance, have been considered. In the method of images the system formed by the source, the array of cylinders and the ground is equivalent to a doubled system source-array of cylinders completely symmetric with respect to the axis defined by the ground.

The self-consistent method presented here is completely general, i.e. independent of the impedance model chosen to characterize the ground, so that different ways to determine the ground impedance can be combined with our semi-analytical model. Here we have used a two-parameter impedance method [19] due to both the simplicity of the model and the good agreement of the results with the experimental data obtained, although this method is constrained for the low grazing angles.

The paper is organized as follows: in section 2, we explain the preliminary conditions of our work, including a brief explanation of both the method of images and the impedance model chosen to characterize the ground. In section 3, we develop the semi-analytical method to model the SC–ground interaction, comparing the results of canonical situations with those obtained with numerical predictions (finite elements method). In section 4, we present the results of the SC–ground interaction as well as the comparison with the experimental data. Finally, in section 5, the concluding remarks of our work are shown.

2. Preliminary conditions: method of images and ground impedance

The most interesting situation in the SC–ground interaction is likely to involve periodic vertical finite cylinder arrays, but this would require the solution of a 3D problem considering the interaction between finite vertical cylinders and the finite impedance ground. Due to the complexity of the geometry of this general problem, the analytical study could be very complicated and the numerical simulations could require long computational time. Here we have considered the more tractable 2D problem involving a periodic array of cylinders with their axes parallel to the ground (horizontal cylinders). This geometry has recently been used to observe BGs for water waves propagating over an infinite periodic array of submerged horizontal circular cylinders in deep water [20].

2.1. Defining the problem. Method of images

Consider a line source placed at point O and an array of M circular scatterers placed in the positive half-space which is air, characterized by the sound velocity, $c = 344\,\mathrm{m\,s^{-1}}$, and density $\rho = 1.23\,\mathrm{kg\,m^{-3}}$. The position of each scatterer C_m, $m = 1, \ldots, M$ is given by the vector $\vec{R}_m$. Figure 1(*a*) shows the scheme of the problem in the particular case of scatterers arranged in a square lattice which is defined by the lattice constant a. The nearest base of the array of scatterers is placed at a distance H_x from the ground, while the nearest vertical base of the array from the source is placed at a distance H_y (see figure 1(*a*))

The geometry used to perform the method of images in our approach is shown in figure 1(*b*). In this approach one should consider the image of the source as well as of the scatterers. Note that all the waves reflected on the ground can be described as waves coming either from the image source or from the image scatterers, then the images are also interacting with the real space. The image source is placed at point O' (from now

on, the image vectors will be characterized by a prime), and the image of scatterers C'_m are placed on the negative half-space. All the vectors measured from the image source are characterized by a prime ($'$).

In the scattering problem, the image of the source and the scatterers should be modulated by the presence of the ground. Next, an amplitude and a phase should be added to correct the contribution of images to the scattered field. Then, as we will see in the next section, the complex reflection coefficient should be considered to perform this correction.

2.2. Ground effect

In some cases the surface of the ground can be considered perfectly rigid (or totally reflective). However, some cases exist, as for example concrete or soil surfaces with or without vegetation, in which there is absorption of energy of the incident acoustic waves. An accurate prediction of the influence of the ground in the scattering produced in the structure requires the knowledge of the absorptive and reflective properties (the acoustic impedance) of the surface. Motivated by previous works [18], we characterize in this work the effect of the ground on the scattering problem using the reflection coefficient $R(\vec{r}_O, \vec{r}_R; \nu)$. In general, $R(\vec{r}_O, \vec{r}_R; \nu)$ is a function that mainly depends on the impedance contrast between the two half-spaces separated by the ground surface, on the frequency (ν) and on the positions of both the source ($\vec{r}_O$) and the receiver ($\vec{r}_C$) by means of the angle of incidence on the ground.

The ground surface itself also provides a significant path for transmission of acoustic energy, particularly at low grazing angles and low frequencies. Incident acoustic energy is transformed into vibrational energy and is transmitted along the surface layer. This vibration disturbance can propagate through long distances, before it is dissipated or re-radiated as sound. At these long distances, the transmission of low frequency sound can be dominated by this surface wave mechanism. In this work, we are interested in the interaction between the SC and the ground effect. Therefore, we have studied regions near the source and in the regime of the dispersion frequencies of the array (high frequencies). Thus, this transmission mechanism is neglected in this work.

When airborne sound impinges on the ground, part of the wave is transmitted while another is refracted at right angles onto the surface. For our purposes, we have focused our attention on the reflected waves leaving the surface at the angle of incidence, with its amplitude and phase modified by the impedance of the surface. This reflected wave propagates towards the receiver in addition to the direct wave from the source and, depending on their relative phases and amplitudes, they may constructively add or destructively interfere [21–23]. The effect of the ground on the propagating wave is usually called excess attenuation and it can be explained in terms of the existence of two sources: the real one and the image source that models the reflected wave. In this case, the governing equation for pressure p at the receiver, assuming a uniform medium and a line source, in the positive half-space is

$$\begin{aligned} p &= H_0(kr) + R(\vec{r}_O, \vec{r}_R; \nu) H_0(kr') \\ &= H_0(kr) + R_p(\vec{r}_O, \vec{r}_R, \nu) H_0(kr') \\ &\quad + (1 - R_p(\vec{r}_O, \vec{r}_R, \nu)) F H_0(kr') \end{aligned} \tag{1}$$

where R_p is the plane wave coefficient, H_0 is the Hankel function of 0th order and first kind; parameter F is the boundary-loss factor which is a mathematical function of a variable w called the numerical distance. These functions are [19, 21]

$$R_p(\vec{r}_O, \vec{r}_R, \nu) = \frac{\cos\theta - \dfrac{Z_{air}}{Z_{ground}}}{\cos\theta + \dfrac{Z_{air}}{Z_{ground}}} \tag{2}$$

$$F = 1 + \imath\sqrt{\pi}\,\mathrm{w}\,\mathrm{e}^{-\mathrm{w}^2}\,\mathrm{erfc}(-\imath\,\mathrm{w}), \tag{3}$$

where

$$\mathrm{w} = \sqrt{\frac{1}{2}\imath k r_2}\left(\cos\theta + \frac{Z_{air}}{Z_{ground}}\right), \tag{4}$$

where Z_{air} and Z_{ground} are the air and ground impedances respectively, r_2 is the distance between the reflection point and the receiver and θ is the reflection angle measured from the normal of the surface. erfc is the complex complementary error function. Usually, fraction $\beta = Z_{air}/Z_{ground}$ is called the admittance of the homogeneous impedance plane. The reflected angle can be obtained as

$$\theta = \arctan\left(\frac{x - x_O}{y + y_O}\right), \tag{5}$$

where $\vec{r}_O = (x_O, y_O)$ is the position of the source and $\vec{r}_R = (x, y)$ is the position of the receiver point with respect to the origin of coordinates (see figure 1).

The knowledge of the expression of the impedance is necessary in order to account the reflection properties of the surface. In this work we have characterized these type of surfaces (open cell foam layer) using a two-parameter impedance model [19] with flow resistivity $\sigma_e = 4\,\mathrm{kPa\,s\,m^{-2}}$ and porosity at the surface $\alpha_e = 105\,\mathrm{m^{-1}}$, being the impedance of the ground

$$Z_{ground} = \rho c_0\left(0.434\sqrt{\frac{\sigma_e}{\nu}}(1+\imath) + 9.75\imath\frac{\alpha_e}{\nu}\right), \tag{6}$$

where ρ and c_0 are the density and the sound velocity of air, respectively.

3. MST for SC over a finite impedance ground (MSTFIG)

The solution of the appropriate scattering problem satisfies the Helmholtz equation in the half-space that is written in polar coordinates (r, θ) as

$$\Delta p(\vec{r}) + k^2 p(\vec{r}) = 0, \tag{7}$$

where

$$\Delta = \frac{1}{r}\frac{\partial}{\partial r}\left(r\frac{\partial}{\partial r}\right) + \frac{1}{r^2}\frac{\partial^2}{\partial\theta^2},$$

$\vec{r} = r(\cos\theta, \sin\theta)$ is the radius vector, p is the acoustic displacement potential, $k = \omega/c$ and ω is the angular frequency. Equation (7) is solved in conjunction with radiation conditions

$$\frac{\partial p}{\partial r} - \mathrm{i}kp = o(r^{-1/2}), \qquad \text{as } r \to \infty. \tag{8}$$

Given that M disjoint cylindrical scatterers located at the positions $\vec{R}_m = \vec{R}_1, \ldots, \vec{R}_M$ all placed above a surface on the symmetry axis (see figure 1) and a sound source located at point O, one can consider the incident field over the nth scatterer in the presence of both the other $M-1$ scatterers and the ground by taking into account the conditions explained in section 2 about the multiple scattering technique and the method of images.

$$p^n(\vec{r}) = p_0(\vec{r}) + \sum_{j=1, j\neq n}^{M} (p_{\mathrm{s}}^j(\vec{r}) + R(\vec{R}_{\mathrm{O}j}, \vec{r}_{\mathrm{R}}; \nu) p_{\mathrm{s}}^{j'}(\vec{r})), \tag{9}$$

where p_0 is the pressure produced by both the real and the image sources and p_{s}^j and $p_{\mathrm{s}}^{j'}$ are the scattered pressure by the jth cylinder and its image j'th cylinder respectively. Equation (9) defines the interaction between the scattering of the array and the ground, therefore the semi-analytical method shown in this work is called MST for finite impedance ground (MSTFIG). The pressure of the sources can be expressed as

$$p_0(\vec{r}) = H_0(kr) + R(\vec{r}_{\mathrm{O}}, \vec{r}_{\mathrm{R}}; \nu) H_0(kr'), \tag{10}$$

where $\vec{r} = r(\cos\theta, \sin\theta)$ is the vector connecting the real line source and the receiver point and $\vec{r'} = r'(\cos\theta', \sin\theta')$ connects the position of the receiver and the image point source. On the other hand, the scattered pressures produced by the cylinders m and m' can be represented as

$$p_{\mathrm{s}}^m(\vec{r}) = \sum_{l=-\infty}^{\infty} A_l^m H_l^{(1)}(kr_m) \mathrm{e}^{\imath l\theta_m}, \tag{11}$$

$$p_{\mathrm{s}}^{m'}(\vec{r}) = \sum_{l=-\infty}^{\infty} A_l^{m'} R(\vec{R}_{\mathrm{O}m}, \vec{r}_{\mathrm{R}}; \nu) H_l^{(1)}(kr_{m'}) \mathrm{e}^{\imath l\theta_{m'}}, \tag{12}$$

where $\vec{r}_m = r_m(\cos\theta_m, \sin\theta_m)$ is a vector connecting the centre of scatterer C_m and the receiver and $\vec{r}_{m'} = r_{m'}(\cos\theta_{m'}, \sin\theta_{m'})$ connects the receiver with the scatterer image $C_{m'}$. Note that the reflected wave on the cylinder image is produced by the presence of the ground, thus the reflected pressure on the cylinder should be modulated by the reflection coefficient as in the case of the incident wave on the ground.

In order to introduce equations (10), (11) and (12) in equation (9) all the terms must be expressed in the same origin of coordinates. To do so, Graf's addition theorems for the Bessel and Hankel functions are necessary [14, 25]. Thus, pressures p_0 and p_{s} in the reference system centred at nth scatterer are

$$p_0(\vec{r}) = \sum_{l=-\infty}^{\infty} (H_{-l}^{(1)}(kR_n) \mathrm{e}^{-\imath l\theta_{R_n}} + R(\vec{r}_{\mathrm{O}}, \vec{r}_{\mathrm{R}}; \nu) H_{-l}^{(1)}(kR'_n) \mathrm{e}^{-\imath l\theta_{R'_n}}) J_l(kr_n) \mathrm{e}^{\imath l\theta_n}, \tag{13}$$

$$p_{\mathrm{s}}^j(\vec{r}) = \sum_{l=-\infty}^{\infty} (G_m^{jn} + R(\vec{R}_{\mathrm{O}j}, \vec{r}_{\mathrm{R}}; \nu) G_m^{j'n}) J_l(kr_n) \mathrm{e}^{\imath l\theta_n}, \tag{14}$$

$$G_m^{jn} = \sum_{s=-\infty}^{\infty} A_{\mathrm{s}}^j H_{m-s}^{(1)}(kR_{jn}) \mathrm{e}^{\imath(m-s)\theta_{jn}} = \sum_{s=-\infty}^{\infty} A_s^j G_{ms}^{jn}, \tag{15}$$

$$G_m^{j'n} = \sum_{s=-\infty}^{\infty} A_{\mathrm{s}}^{j'} H_{m-s}^{(1)}(kR_{j'n}) \mathrm{e}^{\imath(m-s)\theta_{j'n}} = \sum_{s=-\infty}^{\infty} A_s^{j'} G_{ms}^{j'n}, \tag{16}$$

where vector $\vec{R}_n = R_n(\cos\theta_{R_n}, \sin\theta_{R_n})$ ($\vec{R}'_n = R_n(\cos\theta_{R'_n}, \sin\theta_{R'_n})$) defines the position of scatterer C_n with respect to real (image) line source and vector $\vec{R}_{jn} = R_{jn}(\cos\theta_{jn}, \sin\theta_{jn})$ ($\vec{R}_{j'n} = R_{j'n}(\cos\theta_{j'n}, \sin\theta_{j'n})$) defines the position of scatterer C_j ($C_{j'}$) with respect to scatterer C_n.

Finally, due to the geometry of the problem, we can express the total incident wave over the nth scatterer as

$$p^n(\vec{r}) = \sum_{s=-\infty}^{\infty} B_{\mathrm{s}}^n J_{\mathrm{s}}(kr_n) \mathrm{e}^{\imath s\theta_n}. \tag{17}$$

Introducing equations (13), (14) and (17) in equation (9), one can obtain the following system of equations:

$$B_{\mathrm{s}}^n = S_{\mathrm{s}}^n + \sum_{j=1}^{M} ((1-\delta_{jn}) G_{\mathrm{s}}^{jn} + R(\vec{R}_{\mathrm{O}j}, \vec{r}_{\mathrm{R}}; \nu) G_m^{j'n}), \tag{18}$$

where

$$S_{\mathrm{s}}^n = H_{-l}^{(1)}(kR_n) \mathrm{e}^{-\imath l\theta_{R_n}} + R(\vec{r}_{\mathrm{O}}, \vec{r}_{\mathrm{R}}; \nu) H_{-l}^{(1)}(kR'_n) \mathrm{e}^{-\imath l\theta_{R'_n}}. \tag{19}$$

At this stage B_{s}^n, A_{s}^j and $A_{\mathrm{s}}^{j'}$ are unknown coefficients but they can be related using the boundary conditions on the scatterers and the symmetry of the problem. The boundary conditions at the surface of a rigid cylinder relates B_{s}^j with A_{s}^j and the symmetric condition relates A_{s}^j with $A_{\mathrm{s}}^{j'}$. In our approach we will consider the general boundary condition, i.e. the continuity of both the pressure and the normal velocity across the interface between the scatterers and the surrounding medium. Note that the asymptotical situation, $\rho_n \to \infty$ and $c_n \to \infty$, reproduces the case of rigid scatterers (Neumann boundary conditions).

The boundary conditions in the nth scatterer can be expressed as

$$p_{\mathrm{ext}}|_{\partial\Omega_n} = p_{\mathrm{int}}|_{\partial\Omega_n}, \tag{20}$$

$$\frac{1}{\rho} \frac{\partial p_{\mathrm{ext}}}{\partial n}\bigg|_{\partial\Omega_n} = \frac{1}{\rho_n} \frac{\partial p_{\mathrm{int}}}{\partial n}\bigg|_{\partial\Omega_n}, \tag{21}$$

where $\partial\Omega_n$ is the boundary of the nth scatterer, ρ is the density of the surrounding medium and ρ_n is the density of the nth scatterer.

In order to apply the previous boundary conditions, we have considered that the pressure field inside the nth cylinder can be represented by

$$P_{\mathrm{int}}^n = \sum_{j=-\infty}^{\infty} D_j^n J_j(k_{1n} r_n) \mathrm{e}^{\imath j\theta_n}, \tag{22}$$

where k_{1n} is the wave number inside the nth cylinder.

Using the boundary conditions and the expressions of both the exterior and interior fields in the nth scatterer, we can obtain the following relation:

$$B_j^n = \Gamma_j^n A_j^n, \tag{23}$$

where

$$\Gamma_j^n = \frac{H_j(kb_n)J_n'(kb_n/h_n) - g_n h_n H_j'(kb_n)J_j(kb_n/h_n)}{g_n h_n J_j'(kb_n)J_j(kb_n/h_n) - J_j(kb_n)J_j'(kb_n/h_n)}. \tag{24}$$

Here b_n is the radius of the nth cylinder (in this work the radius of the scatterers takes the same value for all the cylinders, $b_n = b$), $g_n = \rho_1^n/\rho$ is the density ratio, and $h_n = k/k_1^n = c_1^n/c$ is the sound speed ratio for the ith cylinder. Note that if the scatterers are acoustically hard, i.e. $\rho_1 \gg \rho$ and $c_1 \gg c$, then the coefficients Γ_j^n coincides with those obtained with the Neumann boundary conditions,

$$\Gamma_j^n = -\frac{\partial_r H_j(kb_n)}{\partial_r J_j(kb_n)}, \tag{25}$$

where ∂_r is the derivative with respect to polar coordinate r.

The image symmetry can be used to relate A_s^j with $A_s^{j'}$. One has to take into account that $r_{j'} = r_j$ and that $\theta_{j'} = -\theta_j$, then

$$\begin{aligned} p_s^{j'}(\vec{r}) &= R(\vec{R}_{Oj}, \vec{r}_R; \nu) \sum_{l=-\infty}^{\infty} A_l^{j'} H_l^{(1)}(kr_{j'}) e^{\imath l\theta_{j'}} \\ &= R(\vec{R}_{Oj}, \vec{r}_R; \nu) \sum_{l=-\infty}^{\infty} A_l^{j} H_l^{(1)}(kr_{j}) e^{-\imath l\theta_{j'}} \\ &= R(\vec{R}_{Oj}, \vec{r}_R; \nu) \sum_{l=-\infty}^{\infty} A_{-l}^{j} H_{-l}^{(1)}(kr_{j}) e^{\imath l\theta_{j'}} \\ &= R(\vec{R}_{Oj}, \vec{r}_R; \nu) \sum_{l=-\infty}^{\infty} A_{-l}^{j} (-1)^l H_l^{(1)}(kr_{j'}) e^{\imath l\theta_{j'}} \end{aligned} \tag{26}$$

and

$$A_l^{j'} = (-1)^l A_{-l}^j. \tag{27}$$

Introducing equation (24) or (25) in (23) and in (18), the following infinite system of equations is obtained:

$$\begin{aligned} \Gamma_s^n A_s^n = S_s^n + \sum_{j=1}^{M} \sum_{l=-\infty}^{\infty} ((1-\delta_{jn}) G_{sl}^{jn} \\ + (-1)^l R(\vec{R}_{Oj}, \vec{r}_R; \nu) G_{s-l}^{j'n}) A_l^n. \end{aligned} \tag{28}$$

The methodology previously shown is completely analytical, however the coefficients A_s^n should be obtained by properly truncating the previous system, i.e. one should use numerical methods to find the solution of the problem. Thus, strictly speaking the methodology is semi-analytical. The subindices l and s take values from $-L$ to L, therefore the infinite system is truncated to one with $2L+1$ equations. In this work, we have truncated the system using $L = 3$ which produces an error less than 1% with respect to the values obtained with $L = 4$. The total acoustic field obtained using the MSTFIG is

$$\begin{aligned} P(\vec{r}) = H_0(kr) + R(\vec{r}_O, \vec{r}_R; \nu) H_0(kr') \\ + \sum_{m=1}^{M} \sum_{l=-\infty}^{\infty} A_l^m (H_l^{(1)}(kr_m) e^{\imath l\theta_m} \\ + R(\vec{R}_{Oj}, \vec{r}_R; \nu) H_l^{(1)}(kr_{m'}) e^{-\imath l\theta_{m'}}). \end{aligned} \tag{29}$$

Note that the methodology shown here is self-consistent and can be applied to any distribution, periodic or random, of scatterers. On the other hand, the effect of the finite impedance of the ground only depends on the model to calculate this impedance, i.e. on the calculation of the reflection coefficient, not on the MST procedure.

Through this work, we will study the variation of the attenuation properties of a SC with different types of grounds. This variation will be represented using the insertion loss (IL) parameter, calculated as

$$\mathrm{IL} = 20 \log_{10} \frac{|p_0|}{|P|}, \tag{30}$$

where P is calculated using equation (29).

3.1. Acoustically hard and completely absorbent grounds

For this study we have considered a 5×3 square array with lattice constant $a = 0.3$ m and diameter of cylinders $D = 0.25$ m. The distance from the ground to the centres of the lowest cylinders in the array is half of the lattice constant, $H_x = 0.15$ m, so that they are separated from the centre of the cylinders of the image array nearest to the ground by the lattice constant. The distance between the source and the array of scatterers is $H_y = 1$ m, and the site of the receiver is (2.5, 0) m. We analyse in this section, two different types of ground: hard ground ($R(\vec{r}_O, \vec{r}_R; \nu) = 1$) and completely absorbent ground ($R(\vec{r}_O, \vec{r}_R; \nu) = 0$).

When the real source is placed on the origin of coordinates ($O = (0, 0)$), then the image source coincides with the real one and depending on the properties of the ground several interesting possibilities can be analysed. With the source on an acoustically hard ground, the predicted IL spectrum of the array should be equivalent to that predicted for an array of double the size (10×3) in the free field (without ground), whereas in the presence of an completely absorbent ground, the IL should be the same as the initial array, 5×3, in free field. In this section, we use these canonical situations in order to check our semi-analytical method, specifically using the MSTFIG in the case of a SC on a surface (section 3) and the MST in the case of a SC in free field. Additional numerical results based on finite element methods (FEMs) have also been used to validate the MSTFIG.

The application of FEM to unbounded domains, as for example the case of the scattering problems, involves a domain decomposition by introducing an artificial boundary around the obstacle. This artificial boundary consists of a region in which the discretization can be coupled in various ways to some discrete representation of the analytical solution. In this work, we use a region of perfectly matched layers (PMLs) [24] to numerically approximate the Sommerfeld

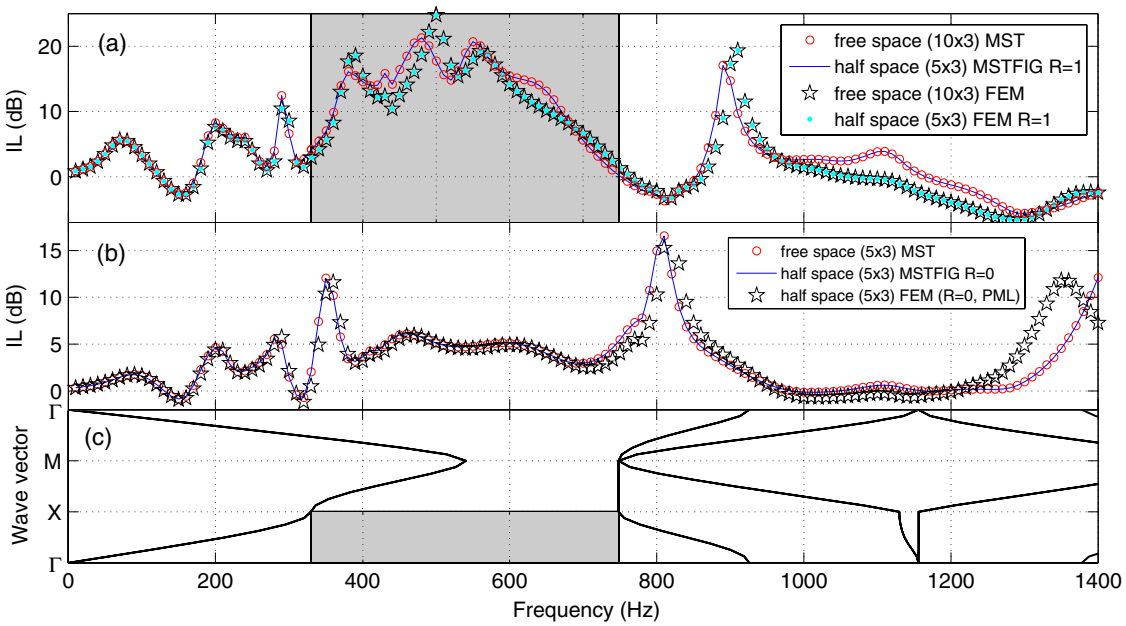

Figure 2. Predicted IL spectra of a square array of rigid cylinders with diameter 0.25 m, lattice constant 0.3 m above ground plane at $y = 0$ and 'lowest' cylinder centres at $H_x = 0.15$ m. The source and receiver coordinates are (0,0) m and (2.5,0) m, respectively. The nearest part of the array is at $H_y = 1$ m from the source. (*a*) Acoustically hard ground $R(\vec{r}_O, \vec{r}_R, \nu) = 1$: blue continuous line, (respectively, green dots) shows the IL produced by a 5×3 square array of rigid cylinders calculated using the MSTFIG (respectively, FEM). The open red circles (respectively, black pentagrams) show the IL produced by a doubled (i.e. a 10×3) lattice in the free field calculated using the MST (respectively, FEM). (*b*) Completely absorbent ground $R(\vec{r}_O, \vec{r}_R, \nu) = 0$: blue continuous line (respectively, open red circles and black pentagrams) shows the IL produced by a 5×3 square array of rigid cylinders calculated using the MSTFIG (respectively, MST and FEM). (*c*) Band structure in the considered case calculated using plane wave expansion (PWE). The grey area represents the pseudogap in the ΓX direction.

conditions (see equation (8)). In this Section the commercial software COMSOL Multiphysics 3.5a is used for the numerical simulations. The PML, originating from electromagnetic computations, is based on simulating an absorbing layer of damping material surrounding the domain of interest, like a thin sponge which absorbs the scattered field radiated on the exterior of this domain. The method was immediately applied to different problems based on the scalar Helmholtz equation as for example acoustics, elasticity, poroelastic media, shallow water waves, etc. Note that MSTFIG gives the pressure field as function of the position, thus one should not solve the entire solution domain to obtain the value at this point. However, FEM should solve the entire solution domain to obtain the value of the field in one point. Thus, FEM takes more computational time than the MSTFIG method to obtain similar convergences.

Figure 2 shows the predicted IL spectra in these two particular cases, acoustically hard and completely absorbent ground. In figure 2(*a*), the acoustically rigid ground is analysed. The blue continuous line shows the IL produced by the array placed on an acoustically hard plane at $y = 0$ calculated using the MSTFIG. The red open circles show the IL produced by a doubled (i.e. a 10×3) lattice in the free field calculated using the MST. The analogous numerical predictions are also shown in figure 2(*a*) with green dots (5×3 square array) and black pentagrams (doubled (i.e. a 10×3) lattice), respectively. Note the complete agreement between both cases, the red open circles completely coincide with the blue line, and the green dots completely coincide with the black pentagram. The possible small differences could be produced by the precision of the mesh in the numerical discretization. The differences in the predictions at higher frequencies can be reduced by considering more elements on the solution domain. However, the computational time is increased.

Figure 2(*c*) represents the band structures for a periodic SC with the same periodicity as the finite structure analysed in this section. These bands have been calculated using the plane wave expansion (PWE) [26]. Grey areas show the pseudogap in the ΓX direction (0° of incidence). The pseudogap covers the range of frequencies (329, 748) Hz. This range is in complete agreement with that obtained using the MSTFIG in the spectra shown in figure 2(*a*). The differences could be produced by the finite size and the near field effects.

In figure 2(*b*), the case of the completely absorbent ground ($R = 0$) with the source at (0,0) is analysed. The blue continuous line shows the IL produced by a 5×3 square array placed on the absorbing ground using the MSTFIG. The red open circles show the IL produced by a 5×3 array in the free field calculated using the MST. The black pentagrams show the FEM predictions. Note the complete agreement between all the cases.

Even though the FEM can be used for analysing the situations studied in this paper, its use has been limited to the purpose of validating the MSTFIG methodology. In the rest of this work we will only use the MSTFIG and we will validate our results with experimental data.

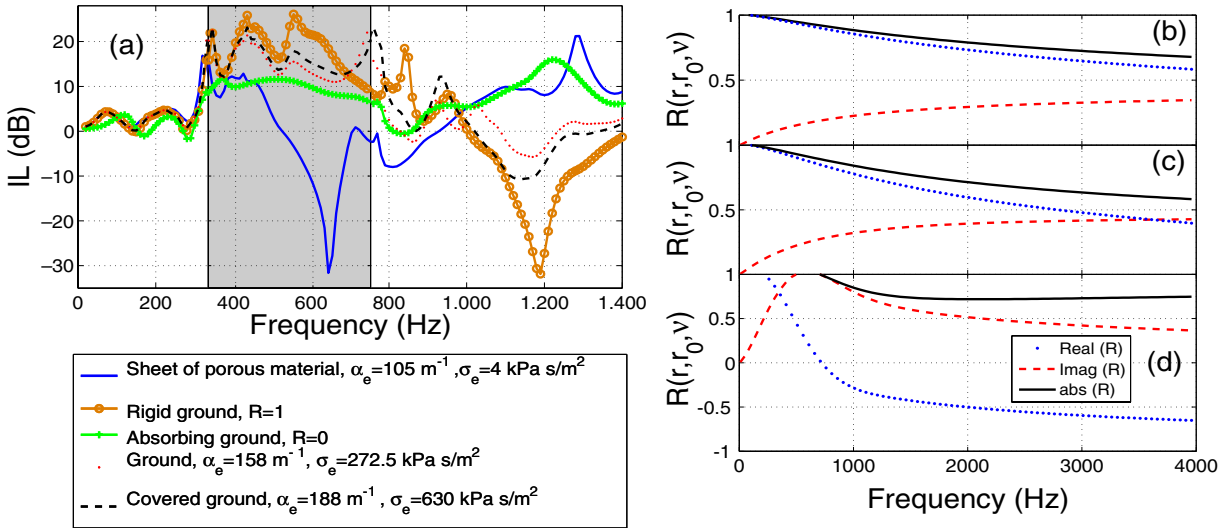

Figure 3. IL and reflection coefficient predictions obtained using the MSTFIG for five values of ground impedance. (*a*) IL of the same array as in figure 2(*a*) with the source and the receiver placed at points (0,0.25) m and (2.5, 0.75) m respectively, and $H_x = 0.15$ m and $H_y = 1$ m. The orange continuous dotted line shows the IL predicted in the case of a rigid ground. The green crossed dash line shows the IL predicted in the case of a completely absorbent ground. The black dashed line shows the IL predictions in the case of a covered ground characterized by $\sigma_e = 630\,\mathrm{kPa\,s\,m^{-2}}$ and $\alpha_e = 188\,\mathrm{m^{-1}}$. Red dots show the IL predicted for the case of a ground characterized by $\sigma_e = 272\,500\,\mathrm{Pa\,s\,m^{-2}}$ and $\alpha_e = 158\,\mathrm{m^{-1}}$. The blue continuous line shows the IL predictions in the case of a sheet of porous material characterized by $\sigma_e = 4000\,\mathrm{Pa\,s\,m^{-2}}$ and $\alpha_e = 105\,\mathrm{m^{-1}}$. The real, imaginary and absolute values of the reflection coefficients of these three grounds are shown in (*b*), (*c*) and (*d*) respectively. The grey area represents the pseudogap in the ΓX direction.

3.2. Finite impedance surface

When the source is not located on the ground, the semi-analytical solution of the problem has to be obtained using the MSTFIG. In the finite impedance surface case we will use experimental data to check the methodology in section 4.3. We analyse here the same array as before but varying the impedance of the ground. As we have previously mentioned, the finite impedances considered here are characterized by a two-parameter impedance model [19] with different values of σ_e and α_e. We have specifically analysed the cases of a rigid ground, a completely absorbent ground, a covered ground characterized in [22], the finite impedance ground analysed in [19] and the sheet of porous material used in this work with $\sigma_e = 4000\,\mathrm{Pa\,s\,m^{-2}}$ and $\alpha_e = 105\,\mathrm{m^{-1}}$.

Figure 3(*a*) shows the IL predictions obtained using the MSTFIG for the five values of the ground impedance. In these cases the source and the receiver are out of the ground, placed at points (0,0.25) m and (2.5, 0.75) m, respectively. Figures 3(*b*)–(*d*) show the absolute, real and imaginary values of the reflection coefficients calculated at the receiver site for the three considered ground impedances. The calculations of these impedances are based on a two-parameter model, being $\sigma_e = 630\,\mathrm{kPa\,s\,m^{-2}}$ and $\alpha_e = 188\,\mathrm{m^{-1}}$, $\sigma_e = 272\,500\,\mathrm{Pa\,s\,m^{-2}}$ and $\alpha_e = 158\,\mathrm{m^{-1}}$, $\sigma_e = 4000\,\mathrm{Pa\,s\,m^{-2}}$ and $\alpha_e = 105\,\mathrm{m^{-1}}$, respectively.

The orange line with open circles in figure 3(*a*) shows the IL of the array over a rigid ground. At around 1200 Hz, the values of the IL are negative because the excess attenuation shows a clear interaction between the BG of the array and the ground effect. Note that this deep in the attenuation spectrum, due to the excess attenuation, depends on the impedance of the ground, thus it could be modelled depending on the considered impedance. The black horizontally dashed line, the red dots, the green vertically dashed and the blue continuous lines show the reduction or shift of the excess attenuation peaks due to the reduction on the reflection coefficient because of the finite ground impedance. Note that the IL is calculated here considering the pressure level of the system with the ground as a reference. Taking this into account, the negativity of the IL means that, although the sound is attenuated behind the SC, the presence of the SC reduces the effect of the excess attenuation peak. This will be discussed in detail in the following sections.

4. Results

In this section, we analyse the effect of the finite ground impedance on the attenuation properties of a periodic array of scatterers from both semi-analytical and experimental points of view. In both cases we have used an array of 7×3 scatterers in square periodicity with lattice constant $a = 0.069$ m over a ground with a line source placed at point $O = (0, 0.235)$ m. The circular scatterers present a radius $r = 0.0275$ m. For these simulations, we have considered $H_y = 0.755$ m and $H_x = 0.0275$ m.

Here, we have considered two different grounds: an acoustically rigid ground ($R = 1$) and a finite impedance ground characterized by a two-parameter model ($\sigma_e = 4000\,\mathrm{Pa\,s\,m^{-2}}$ and $\alpha_e = 105\,\mathrm{m^{-1}}$).

4.1. Symmetry of the acoustic field. Rigid and finite impedance surfaces

In figure 4, we have analysed the symmetry of the acoustic pressure field with respect to the ground plane depending on the value of the impedance. If the impedance is infinite,

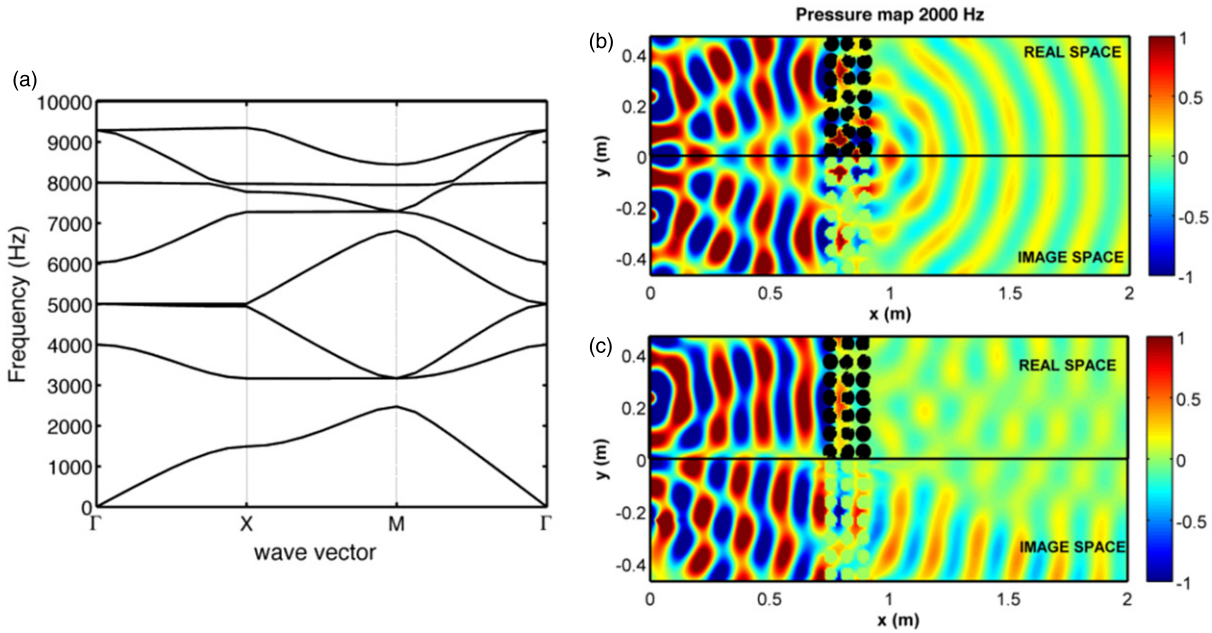

Figure 4. Pressure maps for an array of 7 × 3 scatterers in square array with lattice constant $a = 0.069$ m considering a line source placed at point $O = (0, 0.235)$ m. The circular scatterers present a radius $r = 0.0275$ m. For these simulations we have considered $H_y = 0.755$ m and $H_x = 0.0275$ m. (*a*) Band structure calculated using the PWE method. (*b*) and (*c*) pressure maps ($Re(P)$) (Pa) at 2000 Hz for an acoustically hard ground and an finite impedance ground ($\sigma_e = 4000$ Pa s m^{-2} and $\alpha_e = 105$ m^{-1}), respectively.

i.e. acoustically hard ground, the acoustic field should be symmetric, which means that the acoustic field in the image space should be symmetrically equivalent to the acoustic field in the real space. However, in the case of a finite impedance ground, the symmetry is broken and the field in the real space and the image space are not identical.

Figure 4(*a*) shows the band structure for the considered array calculated using the PWE method. Note that, in this case, the lattice constant is lower than in the previous array, and this produces a shift to higher frequencies of the BG. Moreover, the filling fraction also affects the width of both the pseudogap and the gap. The range of frequencies between 2478 and 3171 Hz defines the full BG for this array. Using the MSTFIG, we have predicted the acoustic field at 2000 Hz considering both an acoustically hard ground and a finite impedance ground. Figures 4(*b*) and (*c*) show the pressure maps ($Re(P)$) at 2000 Hz. One can clearly observe the symmetry of the acoustic pressure field in the hard ground case and how this symmetry is broken in the case of finite impedance.

4.2. BG–ground plane interaction

For a predetermined source position and the impedance of the ground, the IL defined by equation (30) represents the difference between the pressure level measured with and without the array in the presence of the ground. To interpret the IL, one should take into account the effects produced by both the ground and the SC. The ground produces zones with excess attenuation which depends on both the position of the receiver and on the frequency. On the other hand, SC present ranges of attenuated frequencies which depend on both the relative position of the source and the receiver and on the filling fraction. We have calculated the IL spectra using the MSTFIG for the receiver positioned at the interval height $y = [0, 0.469]$ m and for a distance of $x = 1.203$ m from the source. In all these cases the IL has been analysed for the two different kinds of grounds defined at the beginning of this section.

4.2.1. Hard ground. The excess attenuation caused by the ground with the receiver at several heights, due to a rigid ground and without SC, can be observed in figure 5(*a*). Each horizontal cut, $y = y_r$, of the map in figure 5 represents the spectrum at point $(1.203, y_r)$ m. The pressure level (PL) in the receiver sites is characterized with the following expression:

$$\mathrm{PL} = 20 \log_{10}(|H_0(kr) + H_0(kr')|). \tag{31}$$

The excess attenuation appears in figure 5(*a*) as regions of frequencies with negative values of the PL produced by the destructive interference between the incident wave (from the source) and the reflected wave on the ground. Then, the positive values of the PL mean a positive interference and consequently a reinforcement. Figure 5(*a*) shows the dependence of the excess attenuation on the height of the receiver and on the frequency. The higher the height, the lower the frequency of the excess attenuation peak is. Excess attenuation peaks of second order can also be observed for high values of both height and frequencies.

In figure 5(*b*), the IL map produced by the interaction of the rigid ground and the array of scatterers is shown. The vertical dotted line shows the beginning of the pseudogap in the ΓX direction whereas the vertical continuous lines show the range of frequencies of the full BG of the array. This IL is calculated using equation (30). One can observe that, for all the considered heights, the maximum value of IL is obtained for the frequencies inside the pseudogap in thr ΓX direction.

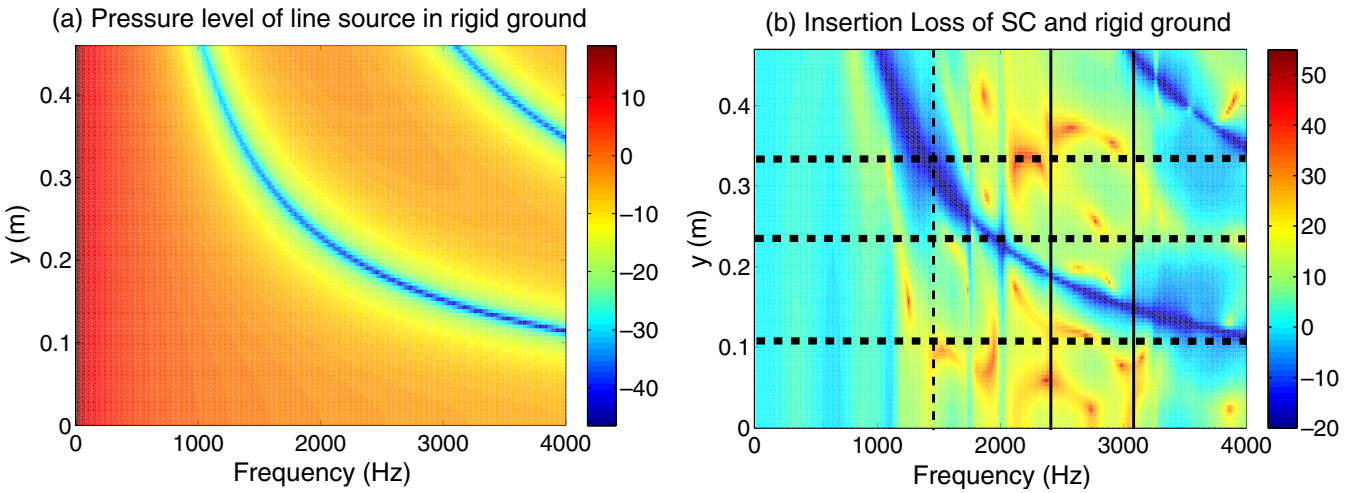

Figure 5. (*a*) Pressure level spectra surface produced by the line source in the presence of a rigid ground. The line source is placed at point $O = (0, 0.235)$ m. We have calculated the pressure level using equation (31) at interval height $y = [0, 0.469]$ m for a distance $x = 1.203$ m from the source. (*b*) IL map produced by a 7×3 array with square periodicity with $a = 0.069$ m. The circular scatterers present a radius $r = 0.0275$. For these simulations we have considered $H_y = 0.755$ m and $H_x = 0.0275$ m. We have calculated the IL spectra using the MSTFIG at interval height $y = [0, 0.469]$ m and for a distance of $x = 1.203$ m from the source. The vertical dashed line marks the beginning of the pseudogap in the ΓX direction (0°) and the vertical continuous line marks the ranges of frequencies of the full BG. The horizontal dotted lines show the semi-analytical and experimental cuts shown in figure 7.

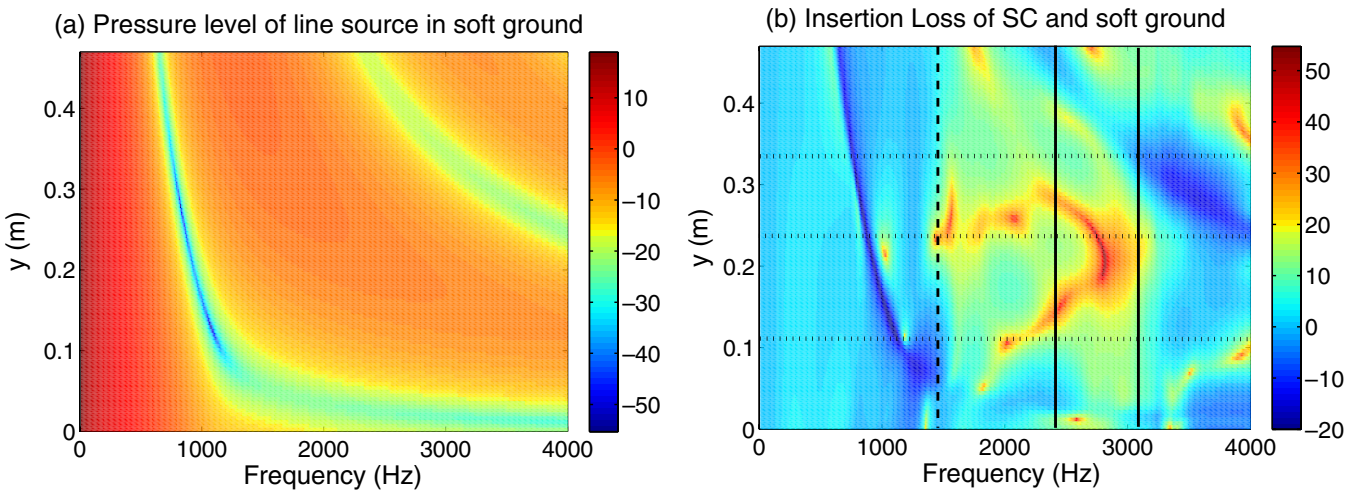

Figure 6. (*a*) Pressure level spectra surface produced by the line source in the presence of a finite impedance ground ($\sigma_e = 4000$ Pa s m^{-2} and $\alpha_e = 105$ m^{-1}). The line source is placed at point $O = (0, 0.235)$ m. We have calculated the pressure level using equation (32) at interval height $y = [0, 0.469]$ m and for a distance of $x = 1.203$ m from the source. (*b*) IL map produced by a 7×3 array with square periodicity with $a = 0.069$ m above a finite impedance ground. The circular scatterers present a radius $r = 0.0275$. For these simulations we have considered $H_y = 0.755$ m and $H_x = 0.0275$ m. We have calculated the IL spectra using the MSTFIG at interval height $y = [0, 0.469]$ m and for a distance of $x = 1.203$ m from the source. The vertical dashed line marks the beginning of the pseudogap in the ΓX direction (0°) and the vertical continuous line marks the ranges of frequencies of the full BG. The horizontal dotted lines show the semi-analytical and experimental cuts shown in figure 8.

However, there are heights at which the IL is negative, which represents a reinforcement with respect to the case in which we used a reflecting surface alone. The low values of the pressure at these points and frequencies for the reference taken to calculate the IL (i.e. the pressure only calculated with the presence of the ground) produce that, although the SC attenuates sound because of the BG, the IL was negative. Then, in comparison with the case of only the ground, the negativity of the IL means that, although at these heights a low pressure level exists, the presence of the SC reduces the excess attenuation of the ground.

4.2.2. Soft ground. The excess attenuation caused by a soft ground ($\sigma_e = 4000$ Pa s m^{-2} and $\alpha_e = 105$ m^{-1}) at different heights of the receiver and without the array of scatterers can be observed in figure 6(*a*). In this case, the pressure level (PL) in the receiver sites is characterized using the following expression:

$$\mathrm{PL} = 20 \log_{10}(|H_0(kr) + R(\vec{r}_O, \vec{r}_R; \nu) H_0(kr')|), \qquad (32)$$

where $R(\vec{r}_O, \vec{r}_R; \nu)$ is calculated using the approach shown in section 2.2 and is obtained by combining equations (2) and (6) in equation (1).

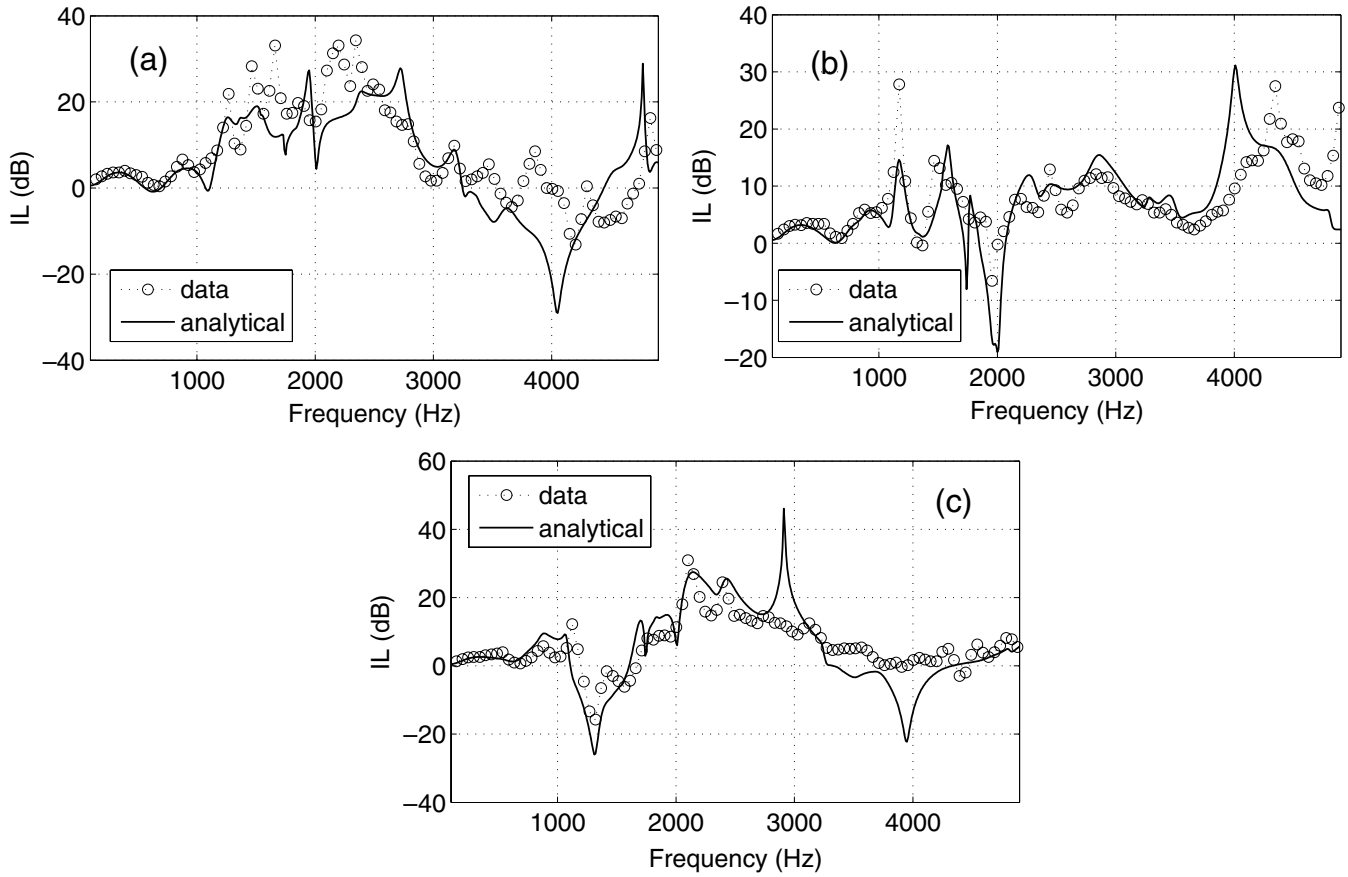

Figure 7. Measured (open circle with dotted line) and predicted (continuous line) insertion loss spectra for a source at coordinates (0,0.235) m and 0.755 m from a 7 × 3 array of rigid cylinders of a 0.055 m diameter over acoustically hard ground with receiver coordinates (*a*) (1.203,0.117) m, (*b*) (1.203,0.235) m and (*c*) (1.203,0.352) m. Arrays of cylinders placed near the ground surface.

In figure 6(*a*), one can observe the pressure level in the case of a sound source with this finite impedance ground. Once again, the excess attenuation also depends on both the frequency and the height of the receiver. However, this dependence changes due to the properties of the ground. The first excess attenuation peak appears at lower frequencies and lower heights than in the case of the acoustically rigid ground. Excess attenuation peaks of second order can also be observed for lower values of both heights and frequencies than in the case of the rigid ground.

Figure 6(*b*) shows the IL maps produced as a result of the interplay between the soft ground and the array of scatterers. The vertical dotted line shows the beginning of the pseudogap in the ΓX direction whereas the continuous lines show the range of frequencies of the full BG of the array. As in the case of the hard ground, the attenuation peaks are once again present due to the influence of the ground. One can also observe that the array of scatterers changes the attenuation properties at the receiver site for frequencies above and below the first peak of excess attenuation adding this effect to that related with the BG.

4.3. Comparisons between data and predictions

4.3.1. Laboratory experiment. 2 m long PVC cylinders with outer diameters of 55 mm have been used to construct the 7×3 square periodic array with lattice constant $a = 0.069$ m. The sound source was a Bruel and Kjaer point source loudspeaker controlled by a Maximum-Length Sequence System Analyzer (MLSSA) enabling the determination of impulse responses. Measurements of the insertion loss (IL) spectra for arrays of cylinders placed near a ground surface in an anechoic chamber have been obtained.

A 0.03 m thick wooden board, large enough to avoid the diffraction at the edges, was used as a hard surface. The loudspeaker point source was positioned at 0.755 m from the array at the height of the horizontal mid-plane of the array (0.23 m above the ground). The height of the receiver microphone was 0.117, 0.235 or 0.352 m and it was placed in a vertical plane at 0.257 m from the back of the array. The receiver heights were chosen to be below, at, and above, the horizontal mid-plane of the array. In all cases, a constant distance between the microphone and the periodic array has been considered, in such a way that the distance between the source and the receiver was $x = 1.203$ m. In this study, we have analysed the properties in the ΓX direction (0°). The attenuation spectra have been obtained from the difference between the sound level recorded at the same point in two different configurations: (*i*) the ground alone and (*ii*) the ground and the periodic array.

4.3.2. Hard ground. Figure 7 compares measured and predicted IL spectra for the considered array placed on a

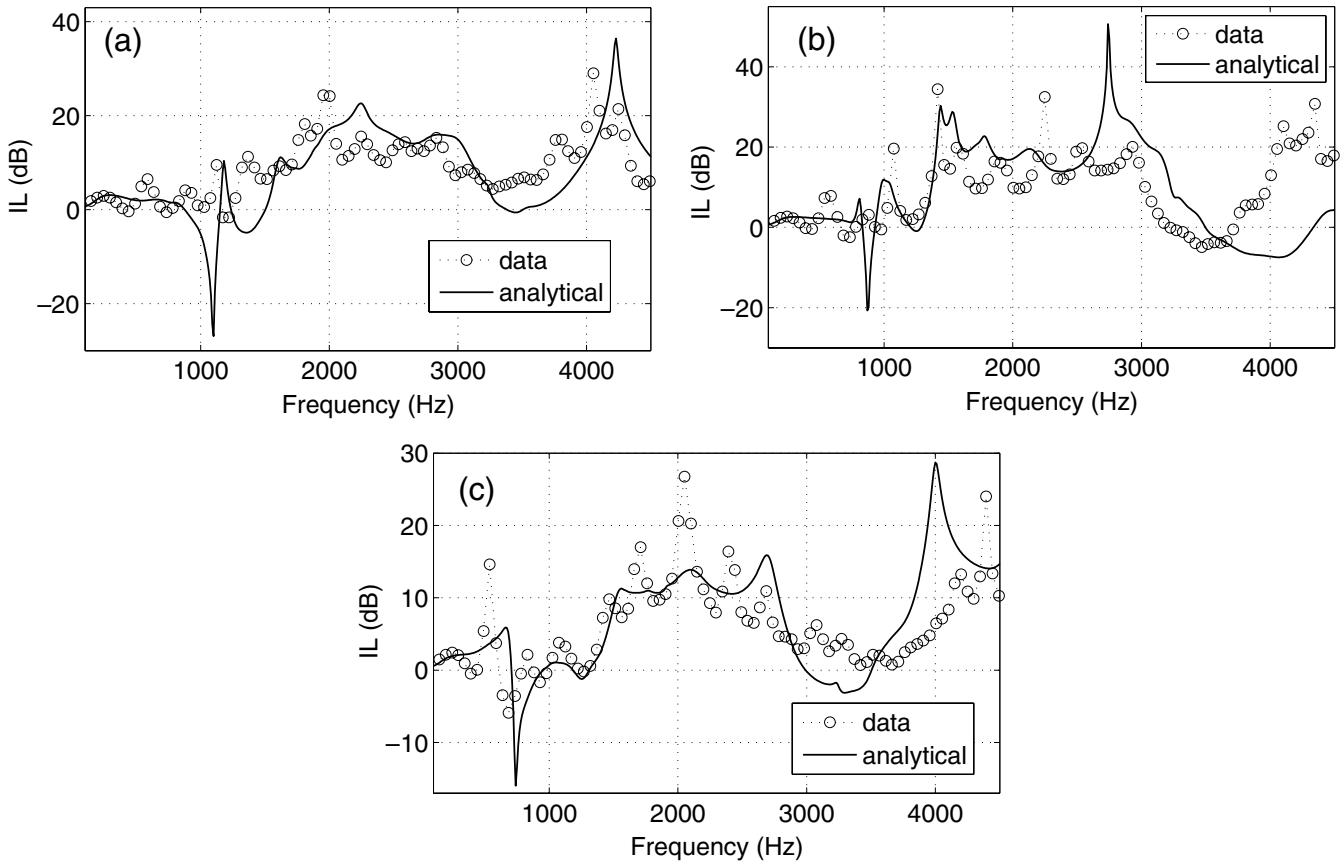

Figure 8. Measured (open circles with line) and predicted (continuous line) insertion loss spectra for a source at coordinates (0,0.235) m and 0.755 m from a 7 × 3 array of rigid cylinders of a 0.055 m diameter over a finite impedance ground with receiver coordinates (*a*) (1.203,0.117) m, (*b*) (1.203,0.235) m and (*c*) (1.203,0.352) m. Arrays of cylinders placed near the ground surface.

hard ground plane with the receiver in three positions with different heights and using the source location described in section 4.3.1. An $R = 1$ value has been used for the calculation due to the rigidity of the ground. The agreement between predictions and measurements is fairly good. The discrepancies observed are probably produced by the fact that the experimental ground is not completely rigid. The semi-analytical spectra corresponding to these three heights are also marked in figure 5(*b*) with dotted horizontal lines. One can observe in figure 7 that the ground effect in the IL due to the excess attenuation peaks for the three heights analysed in this work corresponds with depths at 4000 Hz, 2000 Hz and 1400 Hz respectively. These frequencies correspond to horizontal dotted lines in figure 5(*b*).

In figure 5(*c*), one can observe that the experimental measurements do not reproduce the second order peak of the excess attenuation at high frequencies (4000 Hz). Once again this discrepancy could be due to the fact that the impedance of the ground used in the laboratory is not infinite, i.e. the reflection coefficient is not $R = 1$. However, the agreement between the semi-analytical predictions and the laboratory measurements is good.

4.3.3. Soft ground. Figure 8 compares the corresponding measured and predicted insertion loss spectra for the considered array on a finite impedance ground for the three receiver heights previously described. For the simulations with the MSTFIG we have used the reflection coefficient obtained from equation (2) with the two-parameter impedance model with the values $\sigma_e = 4000\,\mathrm{Pa\,s\,m^{-2}}$ and $\alpha_e = 105\,\mathrm{m^{-1}}$. Once again, the agreement between the predictions and measurements is fairly good. The horizontal dotted lines in figure 6(*b*) show the corresponding cuts of the IL maps for the three heights analysed in this section.

The semi-analytical predictions of the IL spectra in figures 8(*a*) and (*b*) predict excess attenuation peaks around 1000 Hz in complete disagreement with the experimental results. However, in the case of figure 8(*c*), the attenuation peak is well defined both semi-analytically and experimentally. This discrepancy could be explained in terms of the interference between the microphone and the finite impedance ground at low grazing angles. The adverse and the additional attenuation influences of the ground effect in the IL spectra are shifted towards lower frequencies due to the finite impedance of the ground. Note that the dependence of the excess attenuation peak on the height of the receiver produces a lower shift in frequency than in the case of the rigid ground, in complete agreement with the results shown in figure 6(*b*).

5. Concluding remarks

The effect of both rigid and finite impedance grounds on the attenuation properties of an array of rigid cylindrical scatterers has been booth analytically and experimentally analysed. The MST for a SC over a finite impedance ground (MSTFIG) has been developed as a semi-analytical methodology to study the effect of the ground with different values of the impedance on the propagation properties of an array of rigid scatterers in air. We have also analysed the interaction between the SC and the ground with the receiver at different heights. In order to both compare and validate the model, the MSTFIG has been checked with both numerical predictions (FEM) and experimental results obtaining good agreement between them. The excess attenuation produced by the interplay between the sound source and the ground can be used to tune the attenuation properties of the array of scatterers. Then, the excess attenuation should be taken into account in the design of arrays of scatterers acting as SC noise barriers.

Acknowledgments

The authors would like to thank The Open University (UK) for the use of their facilities. This work was supported by the MEC (Spanish Government) and FEDER funds, under Grant No MAT2009-09438.

References

[1] Martínez-Sala R, Sancho J, Sánchez-Pérez J V, Gómez V, Llinares J and Meseguer F 1995 Sound attenuation by sculpture *Nature* **378** 241

[2] Sánchez-Pérez J V, Rubio C, Martínez-Sala R, Sánchez-Grandia R and Gómez V 2002 Acoustic barriers based on periodic arrays of scatterers *Appl. Phys. Lett.* **81** 5240

[3] Sánchez-Dehesa J, Garcia-Chocano V M, Torrent D, Cervera F and Cabrera S 2011 Noise control by sonic crystal barriers made of recycled materials *J. Acous. Soc. Am.* **129** 1173

[4] Krynkin A, Umnova O, Chong A Y B, Taherzadeh S and Attenborough K 2010 Predictions and measurements of sound transmission through a periodic array of elastic shells in air *J. Acoust. Soc. Am.* **128** 3496

[5] Sánchez-Pérez J V, Caballero D, Martínez-Sala R, Rubio C, Sánchez-Dehesa J, Meseguer F, Llinares J and Gálvez F 1998 Sound attenuation by a two-dimensional array of rigid cylinders *Phys. Rev. Lett.* **80** 5325

[6] Liu Z and Zhang X and Mao Y and Zhu Y Y and Yang Z and Chan C T and Sheng P 2000 Locally resonant sonic materials *Science* **289** 1734

[7] Tournat V, Pagneux V, Lafarge D and Jaouen L 2004 Multiple scattering of acoustic waves and porous absorbing media *Phys. Rev.* E **70** 026609

[8] Umnova O, Attenborough K and Linton C M 2006 Effects of porous covering on sound attenuation by periodic arrays of cylinders *J. Acoust. Soc. Am.* **119** 278–84

[9] Romero-García V, Fuster E, Garcia-Raffi L M, Sánchez-Pérez E A, Sopena M, Llinares J and Sánchez-Pérez J V 2006 Band gap creation using quasiordered structures based on sonic crystals *Appl. Phys. Lett.* **88** 174104

[10] Romero-García V, Sánchez-Pérez J V, Garcia-Raffi L M, Herrero J M, García-Nieto S and Blasco X 2009 Hole distribution in phononic crystals: design and optimization *J. Acoust. Soc. Am.* **125** 3774–83

[11] Castiñeira-Ibáñez S, Romero-García V, Sánchez-Pérez J V and Garcia-Raffi L M 2010 Overlapping of acoustic bandgaps using fractal geometries *Eur. Phys. Lett.* **92** 24007

[12] Zaviska F 1913 The deflection of electro magnetic waves on parallel, infinite long orbital cylinder *Ann. Phys.* **40** 1023–56

[13] Linton C M and Evans D V 1990 The interaction of waves with arrays of vertical circular cylinders *J. Fluid Mech.* **215** 549–69

[14] Martin P A 2006 Multiple scattering: interaction of time-harmonic waves with *N* obstacles (Cambridge: Cambridge University Press)

[15] Chen Y Y and Zhen Ye 2001 Theoretical analysis of acoustic stop bands in two-dimensional periodic scattering arrays *Phys. Rev.* E **64** 036616

[16] Boulanger P, Attenborough K, Qin Q and Linton C M 2005 Reflection of sound from random distributions of semi-cylinders on a hard plane: models and data *J. Phys. D: Appl. Phys.* **38** 3480–90

[17] Sainidou R and Stefanou N 2006 Guided and quasiguided elastic waves in phononic crystal slabs *Phys. Rev.* B **73** 184301

[18] Allen J B and Berkley D A 1979 Image method for efficiently simulating small-room acoustics *J. Acoust. Soc. Am.* **65** 943–50

[19] Taherzadeh S and Attenborough K 1999 Deduction of ground impedance from measurements of excess attenuation spectra *J. Acoust. Soc. Am.* **105** 2039–42

[20] Linton C M 2011 Water waves over arrays of horizontal cylinders: band gaps and Bragg resonance *J. Fluid Mech.* **670** 504–26

[21] Piercy J E, Embleton T F W and Sutherland L C 1977 Review of noise propagation in the atmosphere *J. Acoust. Soc. Am.* **61** 1403–18

[22] Attenborough K 1992 Ground parameter information for propagation modeling *J. Acoust. Soc. Am.* **92** 418–27

[23] Attenborough K and Taherzadeh S 1995 Propagation from a point source over a rough finite impedance boundary *J. Acoust. Soc. Am.* **98** 1717–22

[24] Berenguer J P 1994 A perfectly matched layer for the absorption of electromagnetic waves *J. Compt. Phys.* **114** 185

[25] Abramowitz M and Stegun I A 1964 *Handbook of Mathematical Functions* (Washington, CD: National Bureau of Standards) p 255

[26] Kushwaha M, Halevi P, Martínez G, Dobrzynski L and Djafari-Rouhani B 1994 Theory of acoustic band structure of periodic elastic composites *Phys. Rev.* B **49** 2313–22